RESEARCH ARTICLE | NOVEMBER 10 2023

Probing conduction band offsets and confined states at GaAs/GaAsNBi heterointerfaces

T.-Y. Huang ; J. Occena ; C. Greenhill ; T. Borrely ; Y.-C. Yang ; J. Hu ; A. Chen ; C. Zinn ; K. Jenkins ; L. Li ; C. Kurdak ; R. S. Goldman

Appl. Phys. Lett. 123, 192105 (2023)
https://doi.org/10.1063/5.0172295

Probing conduction band offsets and confined states at GaAs/GaAsNBi heterointerfaces

Cite as: Appl. Phys. Lett. **123**, 192105 (2023); doi: 10.1063/5.0172295
Submitted: 14 August 2023 · Accepted: 19 October 2023 ·
Published Online: 10 November 2023

T.-Y. Huang,[1] J. Occena,[1] C. Greenhill,[1] T. Borrely,[3,4] Y.-C. Yang,[1] J. Hu,[1] A. Chen,[1] C. Zinn,[2] K. Jenkins,[2] L. Li,[2,3] C. Kurdak,[2,3] and R. S. Goldman[1,2,3,a)]

AFFILIATIONS

[1]Department of Materials Science and Engineering, University of Michigan, Ann Arbor, Michigan 48109-2136, USA
[2]Applied Physics Program, University of Michigan, Ann Arbor, Michigan 48109-2136, USA
[3]Department of Physics, University of Michigan, Ann Arbor, Michigan 48109-2136, USA
[4]Institute of Physics, University of São Paulo São Paulo 05508-090, Brazil

[a)]**Author to whom correspondence should be addressed:** rsgold@umich.edu

ABSTRACT

We probe the conduction-band offsets (CBOs) and confined states at GaAs/GaAsNBi quantum wells (QWs). Using a combination of capacitance–voltage (C–V) measurements and self-consistent Schrödinger–Poisson simulations based on the effective mass approximation, we identify an N-fraction dependent increase in CBO, consistent with trends predicted by the band anti-crossing model. Using the computed confined electron states in conjunction with photoluminescence spectroscopy data, we show that N mainly influences the conduction band and confined electron states, with a relatively small effect on the valence band and confined hole states in the quaternary QWs. This work provides important insight toward tailoring CBO and confined electron energies, both needed for optimizing infrared optoelectronic devices.

It has been reported that dilute fractions of N and Bi incorporated into GaAs lead to significant bandgap reductions[1–7] while maintaining lattice-matching with GaAs. In particular, it was recently shown that a N:Bi ratio = 0.83 is needed for lattice matching of the quaternary GaAsNBi to GaAs.[8] In addition to this material's promise for infrared detectors and laser diodes,[9–14] solar cells based upon the quaternary GaAsNBi were recently reported.[15]

For GaAsNBi, several theoretical models predict that dilute N fractions lower the GaAs conduction band edge (CBE), while dilute Bi fractions raise the GaAs valence band edge (VBE), both on the order of 100 meV for every 1% N or Bi.[16–21] Thus, co-incorporation of N and Bi is expected to enable independent control of the conduction-band offset (CBO) and valence-band offset (VBO) with respect to GaAs. Beyond computational studies, both C–V measurements and THz spectroscopy have been used to quantify the CBO and VBO of the ternaries. For example, CV measurements of $GaAs_{0.97}N_{0.03}$/GaAs reveal a CBO of 400 ± 10 and a VBO of 11 ± 2 meV,[22,23] and electroreflectance measurements of GaAsN thin films and multi-quantum wells (MQWs) reveal a CBO/ΔE_g of 0.85.[24] In addition, THz spectroscopy of $GaAs_{1-y}Bi_y$/GaAs suggests that CBOs range from 90 to 210 meV and VBOs range from 130 to 530 meV for y_{Bi} from 0.03 to 0.117.[4] To date, measurements of the CBO and VBO for the quaternary $GaAs_{1-x-y}N_xBi_y$/GaAs have not been reported.

Here, we report on the N-fraction dependence CBOs and confined states at GaAs/$GaAs_{1-x}N_x$ and GaAs/$GaAs_{1-x-y}N_xBi_y$ single QWs. We use carrier concentration profiles from C–V data and confinement energies from photoluminescence (PL) spectroscopy, in conjunction with Schrödinger–Poisson simulations of the energy band profiles, to extract the CBOs and confined electron and hole states at the QW interfaces. This work provides important insight into tailoring the CBO, the VBO, and the confined state energies, all critical parameters for performance of quaternary infrared devices.

For this study, we prepared a series of QWs and reference samples by molecular-beam epitaxy. Ternary GaAsN and quaternary GaAsNBi QW were sandwiched between GaAs:Si layers (300 and 690 nm), as shown in Fig. 1. To probe the CBOs and confined state energies, QW thicknesses of 10 nm were targeted to achieve a two-dimensional electron gas (2DEG) with single sub-band occupancy. Confirmation of the 2DEG was achieved via temperature-dependence measurements of capacitance and dissipation, as described in the supplementary material. As shown in the scanning transmission electron microscopy (STEM) image in Fig. 2(a), energy-dispersive x-ray

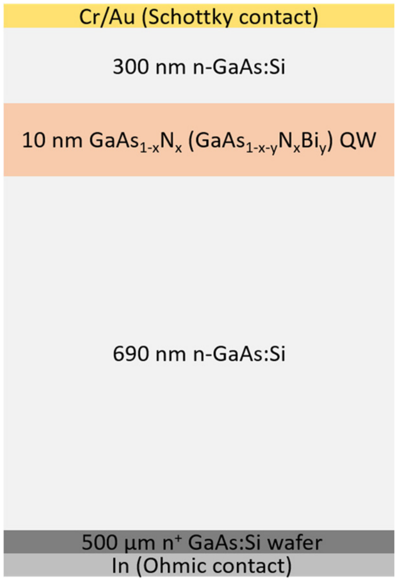

FIG. 1. Sample structure for GaAsN and GaAsNBi QWs. 10 nm ternary GaAsN and quaternary GaAsNBi QW were sandwiched between GaAs:Si layers (300 and 690 nm). Following MBE growth, chrome/gold (200/2000 Å) Schottky contacts were evaporated through a shadow mask with 680 μm diameter circular openings.

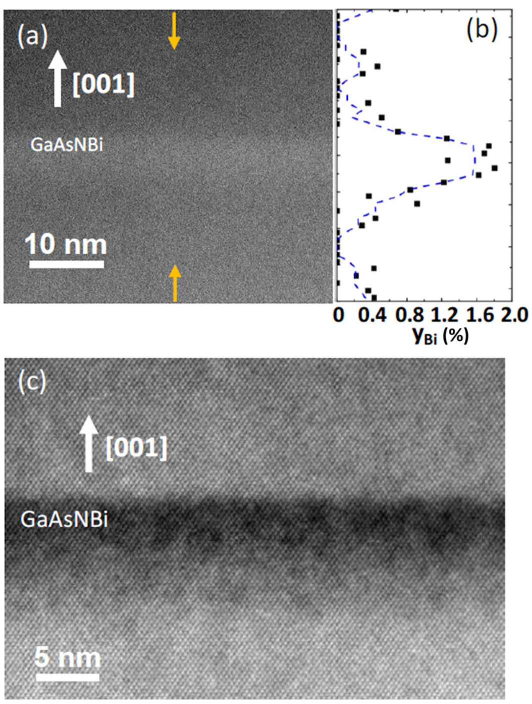

FIG. 2. (a) Scanning transmission electron microscopy (STEM) image, (b) line-cut energy-dispersive x-ray spectroscopy (EDS) data, and (c) cross-sectional transmission electron microscopy image of 10 nm quaternary QW. In (b) and (c), a graded lower interface and an abrupt upper interface are apparent. The black squares in (b) are the EDS data points, showing a maximum $y_{Bi} = 0.018$; and the blue dashed line is the boxcar averaging of the EDS data.

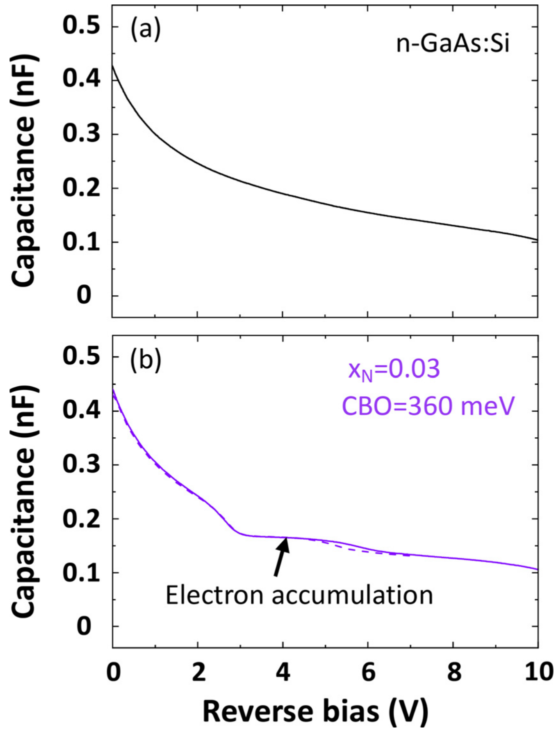

FIG. 3. C–V data for (a) the GaAs:Si reference and (b) the GaAsN QW. In (b), the solid curves correspond to C–V data, while the dashed line corresponds to in next-nano computations, with CBO = 360 meV. For reference sample (a), the capacitance monotonically decreases from ~0.4 to ~0.1 nF as the bias voltage sweeps from 0 to 10 V. For GaAsN QW in (b), a platform-like feature, indicated by an upward arrow, is apparent, due to the electron accumulation in the QW regions.

spectroscopy (EDS) in Fig. 2(b), and the cross-sectional TEM image in Fig. 2(c), the 10 nm quaternary QW has a graded lower interface and an abrupt upper interface with maximum $y_{Bi} = 0.018$, likely due to Bi surface segregation during epitaxy.[25–27] The reference samples consisted of GaAs:Si, $GaAs_{1-x}N_x$, and $GaAs_{1-x-y}N_xBi_y$ films. N mole fractions of $x_N = 0.03$ (GaAsN) and $x_N = 0.007$, 0.019, and 0.024 (GaAsNBi) were determined using x-ray rocking curves in conjunction with nuclear reaction analysis as described in Ref. 28.

Room temperature C–V measurements were conducted using a Keithley 4200 semiconductor parameter analyzer with AC voltage = 30 mV, frequency = 1 MHz, and DC bias swept from 0.5 to −10 V. For comparison, the measured and computed carrier concentration, $\hat{n}$, at a depth z from the Schottky contact were calculated using the depletion approximation:

$$z = \frac{K_s \varepsilon_0 A}{C}, \tag{1}$$

$$\hat{n}(z) = -\frac{2}{q K_s \varepsilon_0 A^2 d(1/C^2)/dV}, \tag{2}$$

where K_s is the GaAs dielectric constant, ε_0 is the permittivity of free space, A is the contact area, q is the elementary charge, and V is the DC reverse bias.

For the $GaAs_{1-x-y}N_xBi_y$ QW, PL spectra were collected at 4.25 K using a 532 nm continuous-wave laser with excitation power of 5 mW.

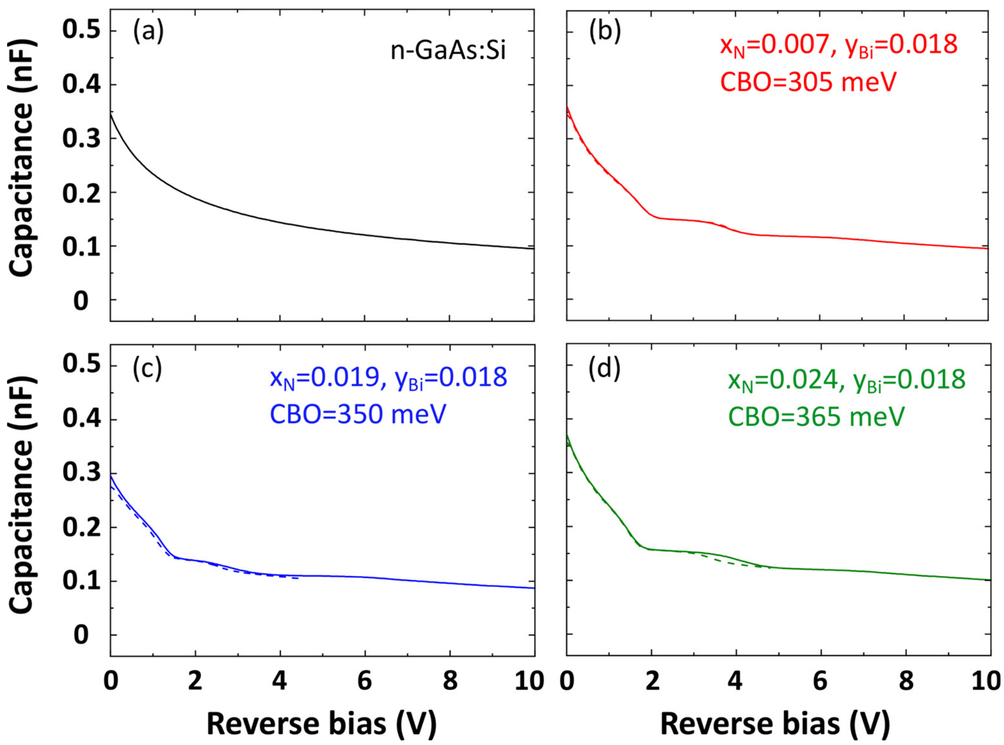

FIG. 4. C–V data for (a) the GaAs:Si reference and (b)–(d) the GaAsNBi QWs. In (b)–(d), the solid curves correspond to C–V data while the dashed lines correspond to nextnano computations, with CBO = 305, 350, and 365 meV. For the reference sample in (a), the capacitance monotonically decreases from ∼0.35 to ∼0.1 nF with bias voltage from 0 to 10 V. For the GaAsNBi QWs in (b)–(d), the platform-like features are apparent in voltage ranging from 2 to 4 V.

Subsequently, the Varshni model was used to estimate the PL emission energy at 300 K

$$E_g(T) = E_g(0) - \frac{\alpha T^2}{\beta + T}, \tag{3}$$

where $\alpha = 4.3\text{–}6.8 \times 10^{-4}$ eV/K and $\beta = 119\text{–}378$ K.[29]

Capacitance–voltage profiles for (a) the GaAs:Si reference and (b) the GaAsN QW are presented in Fig. 3. As the bias is swept from 0 to 10 V, the capacitance decreases from ∼0.4 to ∼0.1 nF. For the reference samples, the capacitance decreases monotonically with increasing reverse bias voltage. For reverse biases in the range of 3–5 V, a platform-like feature, indicated by an upward arrow, is likely due to electron accumulation in the QW.[30,31] Similar platform-like features are observed in the C–V data shown in Fig. 4 for (a) the GaAs:Si reference sample and (b)–(d) the GaAsNBi QWs. The C–V data in Figs. 3 and 4 was converted to electron density vs depth using Eqs. (1) and (2), with an emphasis on the vicinity of the QW, resulting in the plots shown in Fig. 5.

To quantify the CBOs, we compare the C–V-determined electron density profiles with those computed using 1D Schrödinger–Poisson simulations in the effective mass approximation using nextnano. To extract the best fit values of the CBO and fixed charges, we performed a sensitivity analysis, as described in the supplementary material. For GaAsN/GaAs QW, our resulting best fit values are CBO = 360 ± 40 meV and interfacial fixed charge = -6.65×10^{11} |e|/cm^2, as shown in Fig. 5(a). The CBO value is consistent with 400 ± 10 meV reported for a $GaAs_{0.97}N_{0.03}$/GaAs QW[23] and 349 meV interpolated from electroreflectance measurements of GaAsN films and QWs.[24]

For the quaternary QWs with x_N = 0.7%, 1.9%, and 2.4%, y_{Bi} = 1.8%, the measured and simulated electron density and conduction band (CB) edge profiles are shown in Figs. 5(b)–5(d). In this case, the Bi segregation in the quaternary layers is modeled as step-like CBE profiles, and a similar sensitivity analysis is utilized to determine the best fit values for the CBOs and the fixed charges. The CBO values range from 305 ± 10 to 365 ± 30 meV with interfacial fixed charges ranging from −3 to -5.5×10^{11} |e|/cm^2. The trend of increasing CBO with x_N value is consistent with predicted trends. However, the specific CBO values exceed those predicted by the band-anticrossing (BAC)[18,19] and the linear combination of isolated nitrogen resonant states (LCINS) models.[32] Indeed, the layers likely include N configurations that are not accounted for in the BAC and LCINS models, such as N–As or N–N pairs sitting on an arsenic site, termed "split interstitials." These split interstitials may contribute to a reduced effective bandgap of GaAsN and GaAs(N)Bi.

The 4.25 K PL spectra for quaternary QWs are shown in Fig. 6(a). For all three quaternary QWs, emissions in the range of 1.18–1.22 eV, labeled "E_o," are the effective band gaps and attributed to recombination from the confined electron ($E^1{}_e$),

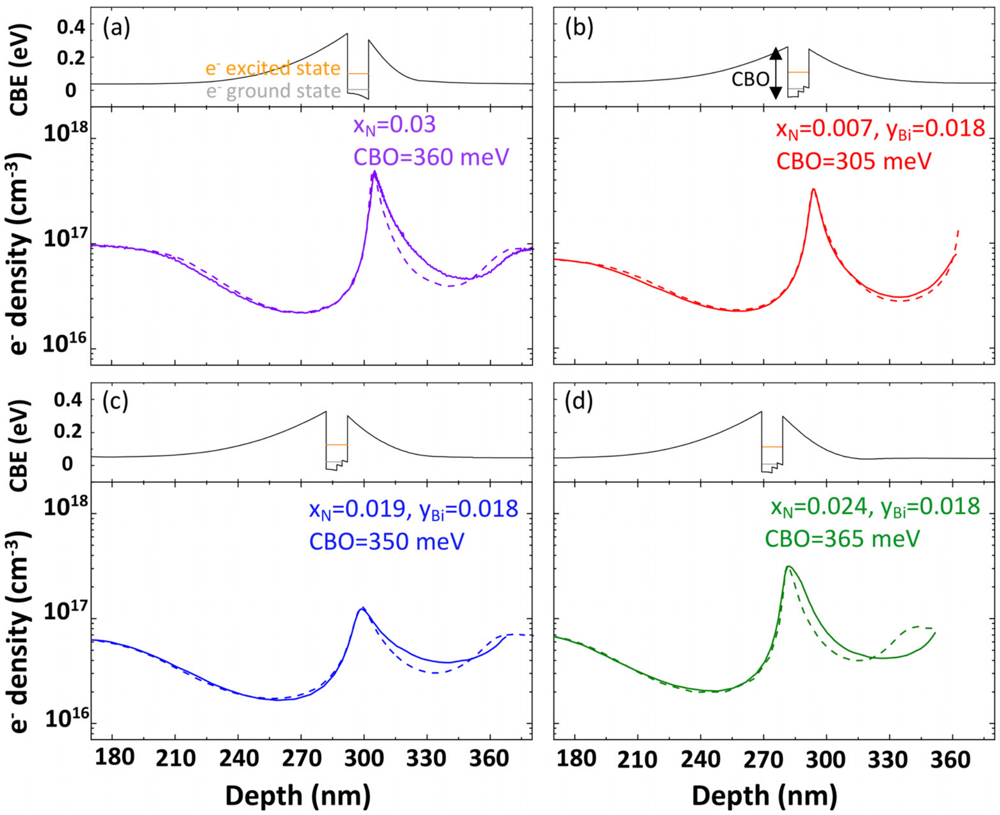

FIG. 5. CBE and electron density vs depth profiles for (a) the ternary GaAsN QW and (b)–(d) the quaternary GaAsNBi QWs. The solid curves correspond to the C–V data, while the dashed lines correspond to nextnano computations using the listed CBO values. In all cases, the electron ground states and first excited states in the QWs are indicated by the solid gray and orange lines, respectively. For (b)–(d), the Bi segregation in the quaternary layers are modeled as step-like CBE profiles.

hole ground states (E_h). In addition, the higher energy emissions at ~1.35 eV, labeled "E_1," are attributed to recombination from the first excited electron (E^2_e) and E_h. For the quaternary QW with the lowest x_N, a localized N-related state lies within the bandgap, resulting in the ~1.06 eV emission labeled "E_N."[33–36] For the quaternary QWs with higher x_N values as the CB edge is lowered, the intensity of emission from the N-localized states is decreased,[21] similar to the Bi-states in valence band.[37]

To determine the positions of the hole ground states, we combine the CBOs and E^1_e from C–V data and nextnano simulations with the Varshni-model estimates of room temperature PL emission energies. The values of E_h are calculated by $E_{gGaAs} - E^1_e - E_o$, as shown in Fig. 6(b). Table I presents the CBOs, room temperature PL emission energies, the values of E_h, and the energy difference between electron ground states and first excited electron states ($E^1_e - E^2_e$). The values of E_h show a relatively weak dependence on N fraction, consistent with earlier reports for GaAsN QWs, MQWs, and thin films that suggest a relatively small VBO compared to CBO.[22–24,38] Thus, for GaAsNBi, N mainly influences the values of the CB, E^1_e, with a relatively small effect on the values of valence band (VB) and E_h. Finally, $E^2_e - E^1_e$ is 100–110 meV, comparable to the value of $E_1 - E_o$ (110–170 meV), suggesting that E_1 is due to the recombination from the first excited electron and the hole ground states.

TABLE I. Conduction band offset (ΔE_c), confined electron energy (E^1_e), confined hole energy (E_h), effective bandgap (E_o), and energy of N-related (E_N) with respect to the conduction band edge of GaAs. $E^2_e - E^1_e$ is 100–110 meV, comparable to the value of E_1-E_o (110–170 meV), suggesting that E_1 is due to recombination from E^2_e and E_h. Note that "E_o Varshni @RT" and "E_1 Varshni @ RT" are Varshni-model estimates of room temperature values of E_o and E_1.

x_N (NRA)	y_{Bi} (EDS)	ΔE_c (eV) (C–V)	E_N (eV) PL @4.25 K	E_o (eV) PL @4.25 K	E_o (eV) Varshni @RT	E_1 (eV) PL @4.25 K	E_1 (eV) Varshni @RT	E^1_e (eV) (nextnano)	E_h (eV)	$E^2_e - E^1_e$ (eV) (nextnano)
0.7%	1.8%	0.305	1.06	1.22	1.14	1.34	1.25	0.247	0.04	0.1
1.9%	1.8%	0.35	0.98	1.18	1.1	1.36	1.27	0.292	0.03	0.1
2.4%	1.8%	0.365	0.97	1.18	1.1	1.36	1.27	0.303	0.02	0.11

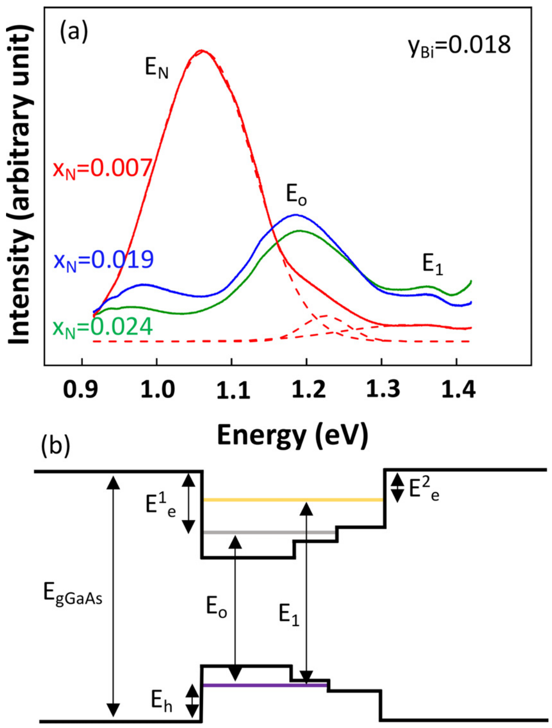

FIG. 6. (a) 4.25 K PL spectra of quaternary GaAsNBi QWs and (b) band-line-ups for GaAsNBi QWs. In (a), emissions in the range 1.18–1.22 eV, labeled "E_o," are effective bandgaps and attributed to recombination from E^1_e and E_h. The higher energy emissions at ~1.35 eV, labeled "E_1," are attributed to recombination from the E^2_e and E_h. For the quaternary QW with the lowest x_N, a localized N-related state lies within the bandgap, resulting in the ~1.06 eV emission labeled "E_N." The energies of E_{gGaAs}, E^1_e, E^2_e, E_o, E_1, and E_h are shown in (b). The values of E_h are calculated using $E_{gGaAs} - E^1_e - E_o$.

In summary, we have examined the CBO, VBO, and confined state energies for GaAsNBi/GaAs. The trend of increasing CBO with the x_N value is consistent with predicted trends. Meanwhile, the N fraction in GaAsNBi has a relatively small effect on the values of the VB and E_h, consistent with earlier studies of GaAsN. This work provides important insight for tailoring CBOs and confined electron energies for improving infrared optoelectronic device applications.

See the supplementary material for details of epitaxial growth, quantification of compositions and in-plane strains and presentation of evidence for two-dimensional electron gas (2DEG) formation within the QWs. In addition, the key parameters for nextnano simulations, including electron effective masses, conduction band offsets (CBOs) and interfacial fixed charges, and the description of sensitivity analysis for extracting best fit values and error bars of CBOs are included.

We gratefully acknowledge support from the National Science Foundation (Grant No. DMR 1810280). The work at UM Physics was supported by the National Science Foundation under Award No. DMR 2004288 (L.L. capacitance spectroscopy). This study was financed in part by the Coordenação de Aperfeiçoamento de Pessoal de Nível Superior—Brasil (CAPES)—Finance Code 001. T.-Y.H. was supported by the Chia-Lun Lo Fellowship and K.J. was supported by the Rackham Merit Fellowship via the Rackham Graduate School at the University of Michigan.

AUTHOR DECLARATIONS

Conflict of Interest

The authors have no conflicts to disclose.

Author Contributions

Tao-Yu Huang: Conceptualization (lead); Data curation (lead); Formal analysis (lead); Investigation (lead); Methodology (lead); Software (lead); Visualization (lead); Writing – original draft (lead); Writing – review & editing (lead). **Lu Li:** Data curation (equal); Formal analysis (equal); Funding acquisition (equal); Methodology (equal); Project administration (equal); Supervision (equal); Writing – review & editing (equal). **Cagliyan Kurdak:** Conceptualization (equal); Formal analysis (equal); Investigation (equal); Methodology (equal); Project administration (equal); Supervision (equal); Writing – review & editing (equal). **Rachel S. Goldman:** Conceptualization (equal); Formal analysis (equal); Funding acquisition (lead); Methodology (equal); Project administration (lead); Resources (lead); Supervision (lead); Visualization (equal); Writing – original draft (equal); Writing – review & editing (equal). **Jordan Occena:** Conceptualization (equal); Data curation (equal); Formal analysis (equal); Investigation (equal); Methodology (equal). **Christian Greenhill:** Data curation (equal); Formal analysis (equal); Investigation (equal); Methodology (equal); Software (equal); Visualization (equal); Writing – original draft (equal); Writing – review & editing (equal). **Thales Borrely:** Conceptualization (equal); Formal analysis (equal); Investigation (equal); Visualization (equal); Writing – original draft (equal); Writing – review & editing (equal). **Yu-Chen Yang:** Software (equal); Visualization (equal); Writing – review & editing (equal). **Jack Hu:** Conceptualization (equal); Data curation (equal); Formal analysis (equal); Investigation (equal). **Andra Chen:** Data curation (equal); Formal analysis (equal); Investigation (equal). **Cameron Zinn:** Data curation (equal); Formal analysis (equal); Investigation (equal); Methodology (equal); Software (equal). **Kaila Grace Jenkins:** Data curation (equal); Formal analysis (equal); Investigation (equal); Methodology (equal); Writing – review & editing (equal).

DATA AVAILABILITY

The data that support the findings of this study are available within the article and its supplementary material.

REFERENCES

[1] M. Weyers, M. S. M. Sato, and H. A. H. Ando, "Red shift of photoluminescence and absorption in dilute GaAsN alloy layers," Jpn. J. Appl. Phys., Part 2 **31**, L853 (1992).
[2] S. Francoeur, M.-J. Seong, A. Mascarenhas, S. Tixier, M. Adamcyk, and T. Tiedje, "Band gap of $GaAs_{1-x}Bi_x$, 0<x<3.6%," Appl. Phys. Lett. **82**, 3874 (2003).
[3] K. Uesugi, I. Suemune, T. Hasegawa, T. Akutagawa, and T. Nakamura, "Temperature dependence of band gap energies of GaAsN alloys," Appl. Phys. Lett. **76**, 1285 (2000).
[4] V. Karpus, R. Norkus, R. Butkutė, S. Stanionytė, B. Čechavičius, and A. Krotkus, "THz-excitation spectroscopy technique for band-offset determination," Opt. Express **26**, 33807 (2018).
[5] P. Klangtakai, S. Sanorpim, K. Yoodee, W. Ono, F. Nakajima, R. Katayama, and K. Onabe, in *Characterization of MOVPE Grown $GaAs_{1-x}N_x$/GaAs*

Multiple Quantum Wells Emitting Around 1.3-μm-Wavelength Region, 2nd IEEE International Conference on Nano/Micro Engineered and Molecular Systems (IEEE, 2007), p. 701.

[6]Y. Zhang, A. Mascarenhas, H. P. Xin, and C. W. Tu, "Scaling of band-gap reduction in heavily nitrogen doped GaAs," Phys. Rev. B **63**, 161303 (2001).

[7]P. H. Tan, X. D. Luo, Z. Y. Xu, Y. Zhang, A. Mascarenhas, H. P. Xin, C. W. Tu, and W. K. Ge, "Photoluminescence from the nitrogen-perturbed above-bandgap states in dilute $GaAs_{1-x}N_x$ alloys: A microphotoluminescence study," Phys. Rev. B **73**, 205205 (2006).

[8]J. Occena, T. Jen, J. W. Mitchell, W. M. Linhart, E.-M. Pavelescu, R. Kudrawiec, Y. Q. Wang, and R. S. Goldman, "Mapping the composition-dependence of the energy bandgap of GaAsNBi alloys," Appl. Phys. Lett. **115**, 082106 (2019).

[9]M. Yoshimoto, W. Huang, Y. Takehara, K. Oe, A. Chayahara, and Y. Horino, *Molecular beam epitaxy of quaternary semiconductor alloy GaNAsBi*, 16th International Conference on Indium Phosphide and Related Materials (IEEE, 2004), p. 501.

[10]M. Yoshimoto, W. Huang, Y. Takehara, J. Saraie, A. Chayahara, Y. Horino, and K. Oe, "New semiconductor GaNAsBi alloy grown by molecular beam epitaxy," Jpn. J. Appl. Phys, Part 2 **43**, L845 (2004).

[11]W. Huang, M. Yoshimoto, Y. Takehara, J. Saraie, and K. Oe, "$GaN_yAs_{1-x-y}Bi_x$ alloy lattice matched to GaAs with 1.3 μm photoluminescence emission," Jpn. J. Appl. Phys., Part 2 **43**, L1350 (2004).

[12]W. Huang, K. Oe, G. Feng, and M. Yoshimoto, "Molecular-beam epitaxy and characteristics of $GaN_yAs_{1-x-y}Bi_x$," J. Appl. Phys. **98**, 053505 (2005).

[13]M. Yoshimoto, W. Huang, G. Feng, and K. Oe, "New semiconductor alloy GaNAsBi with temperature-insensitive bandgap," Phys. Status Solidi B **243**, 1421–1425 (2006).

[14]G. Feng, K. Oe, and M. Yoshimoto, "Influence of thermal annealing treatment on the luminescence properties of dilute GaNAs–bismide alloy," Jpn. J. Appl. Phys., Part 1 **46**, L764 (2007).

[15]H. Kawata, S. Hasegawa, J. Matsumura, H. Nishinaka, and M. Yoshimoto, "Fabrication of a GaAs/GaNAsBi solar cell and its performance improvement by thermal annealing," Semicond. Sci. Technol. **36**, 095020 (2021).

[16]P. J. Klar, H. Grüning, W. Heimbrodt, J. Koch, W. Stolz, S. Tomić, and E. P. O'Reilly, "Monitoring the non-parabolicity of the conduction band in $GaN_{0.018}As_{0.982}$/GaAs quantum wells," Solid-State Electron. **47**, 437 (2003).

[17]P. J. Klar, H. Grüning, W. Heimbrodt, G. Weiser, J. Koch, K. Volz, W. Stolz, S. W. Koch, S. Tomić, S. A. Choulis, T. J. C. Hosea, E. P. O'Reilly, M. Hofmann, J. Hader, and J. V. Moloney, "Interband transitions of quantum wells and device structures containing Ga(N, As) and (Ga, In)(N, As)," Semicond. Sci. Technol. **17**, 830 (2002).

[18]S. J. Sweeney and S. R. Jin, "Bismide-nitride alloys: Promising for efficient light emitting devices in the near- and mid-infrared," J. Appl. Phys. **113**, 043110 (2013).

[19]N. Ajnef, W. Q. Jemmali, M. M. Habchi, and A. Rebey, "Biaxial strain effects on the band structure and absorption coefficient of $GaAs_{1-x-y}N_xBi_y$/GaAs MQWs calculated using k p method," Optik **223**, 165484 (2020).

[20]M. Usman, C. A. Broderick, and E. P. O'Reilly, "Impact of disorder on the optoelectronic properties of $GaN_yAs_{1-x-y}Bi_x$ alloys and heterostructures," Phys. Rev. Appl. **10**, 044024 (2018).

[21]P. R. C. Kent and A. Zunger, "Theory of electronic structure evolution in GaAsN and GaPN alloys," Phys. Rev. B **64**, 115208 (2001).

[22]P. Krispin, S. G. Spruytte, J. S. Harris, and K. H. Ploog, "Electrical depth profile of p-type GaAs/Ga(As, N)/GaAs heterostructures determined by capacitance–voltage measurements," J Appl. Phys. **88**, 4153 (2000).

[23]P. Krispin, S. G. Spruytte, J. S. Harris, and K. H. Ploog, "Admittance dispersion of n-type GaAs/Ga(As, N)/GaAs heterostructures grown by molecular beam epitaxy," J. Appl. Phys. **90**, 2405 (2001).

[24]Y. Zhang, A. Mascarenhas, H. P. Xin, and C. W. Tu, "Formation of an impurity band and its quantum confinement in heavily doped GaAs:N," Phys. Rev. B **61**, 7479 (2000).

[25]X. Lu, D. A. Beaton, R. B. Lewis, T. Tiedje, and M. B. Whitwick, "Effect of molecular beam epitaxy growth conditions on the Bi content of $GaAs_{1-x}Bi_x$," Appl. Phys. Lett. **92**, 192110 (2008).

[26]R. B. Lewis, M. Masnadi-Shirazi, and T. Tiedje, "Growth of high Bi concentration $GaAs_{1-x}Bi_x$ by molecular beam epitaxy," Appl. Phys. Lett. **101**, 082112 (2012).

[27]D. A. Beaton, A. Mascarenhas, and K. Alberi, "Insight into the epitaxial growth of high optical quality $GaAs_{1-x}Bi_x$," J. Appl. Phys. **118**, 235701 (2015).

[28]J. Occena, T. Jen, E. E. Rizzi, T. M. Johnson, J. Horwath, Y. Q. Wang, and R. S. Goldman, "Bi-enhanced N incorporation in GaAsNBi alloys," Appl. Phys. Lett. **110**, 242102 (2017).

[29]W. Żuraw, W. M. Linhart, J. Occena, T. Jen, J. W. Mitchell, R. S. Goldman, and R. Kudrawiec, "Temperature-dependent study of $GaAs_{1-x-y}N_xBi_y$ alloys for band-gap engineering: Photoreflectance and k p modeling," Appl. Phys. Express **13**, 091005 (2020).

[30]C. R. Moon, B.-D. Choe, S. D. Kwon, H. K. Shin, and H. Lim, "Electron distribution and capacitance–voltage characteristics of n-doped quantum wells," J. Appl. Phys. **84**, 2673 (1998).

[31]B. M. Tschirner, F. Morier-Genoud, D. Martin, and F. K. Reinhart, "Capacitance-voltage profiling of quantum well structures," J. Appl. Phys. **79**, 7005 (1996).

[32]E. P. O'Reilly, A. Lindsay, and S. Fahy, "Theory of the electronic structure of dilute nitride alloys: Beyond the band-anti-crossing model," J. Phys.: Condens. Matter **16**, S3257 (2004).

[33]J. F. Chen, C. T. Ke, P. C. Hsieh, C. H. Chiang, W. I. Lee, and S. C. Lee, "Deep-level emissions in GaAsN/GaAs structures grown by metal organic chemical vapor deposition," J. Appl. Phys. **101**, 123515 (2007).

[34]D. Sentosa, T. Xiaohong, and C. S. Jin, "Luminescence from the deep level N–N interstitials in GaAsN grown by metal organic chemical vapour deposition," CrystEngComm **12**(7), 2153–2156 (2010).

[35]M.-C. Hsieh, J.-F. Wang, Y.-S. Wang, C.-H. Yang, C.-H. Chiang, and J.-F. Chen, "Electron emission properties of GaAsN/GaAs quantum well containing N-related localized states: The influence of illuminance," Jpn. J. Appl. Phys., Part 1 **51**, 02BJ12 (2012).

[36]F. Hassen, Z. Zaaboub, M. Bouhlel, M. Naffouti, H. Maaref, and N. M. Garni, "Optical characterization and carriers transfer between localized and delocalized states in Si-doped GaAsN/GaAs epilayer," Thin Solid Films **594**, 168 (2015).

[37]O. Donmez, A. Erol, M. C. Arikan, H. Makhloufi, A. Arnoult, and C. Fontaine, "Optical properties of GaBiAs single quantum well structures grown by MBE," Semicond. Sci. Technol. **30**, 094016 (2015).

[38]R. Kudrawiec, M. Motyka, M. Gladysiewicz, J. Misiewicz, J. A. Gupta, and G. C. Aers, "Contactless electroreflectance of GaN_yAs_{1-y}/GaAs multi quantum wells: The conduction band offset and electron effective mass issues," Solid State Commun. **138**, 365 (2006).